Discussion of "transverse Nonuniformity of Air-Water Flow and Lateral Wall Effects in Quasi-Two-Dimensional Hydraulic Jump"

Wuthrich, Davide; Shi, Rui; Chanson, Hubert

DOI
10.1061/JIDEDH.IRENG-10047

Publication date
2023

Document Version
Final published version

Published in
Journal of Irrigation and Drainage Engineering

Citation (APA)
Wuthrich, D., Shi, R., & Chanson, H. (2023). Discussion of "transverse Nonuniformity of Air-Water Flow and Lateral Wall Effects in Quasi-Two-Dimensional Hydraulic Jump". *Journal of Irrigation and Drainage Engineering*, *149*(4), Article 07023004. https://doi.org/10.1061/JIDEDH.IRENG-10047

Discussion of "Transverse Nonuniformity of Air–Water Flow and Lateral Wall Effects in Quasi-Two-Dimensional Hydraulic Jump"

Davide Wűthrich

Assistant Professor, Dept. of Hydraulic Engineering, Delft Univ. of Technology, Delft 2628 CN, Netherlands. ORCID: https://orcid.org/0000-0003-1974-3560.

Rui Shi

Research Fellow, School of Civil Engineering, Univ. of Queensland, Brisbane, QLD 4072, Australia.

Hubert Chanson

Professor, Hydraulic Engineering, Univ. of Queensland, School of Civil Engineering, Brisbane QLD 4072, Australia (corresponding author). ORCID: https://orcid.org/0000-0002-2016-9650. Email: h.chanson@uq.edu.au

This paper presents a discussion of "Transverse Nonuniformity of Air–Water Flow and Lateral Wall Effects in Quasi-Two-Dimensional Hydraulic Jump" by Rongcai Tang, Jingmei Zhang, Ruidi Bai, and Hang Wang. https://doi.org/10.1061/(ASCE)IR.1943-4774.0001697.

The original article presented a challenging and worthwhile data set on hydraulic jumps with high inflow Froude numbers. It discussed a number of very relevant considerations linked to transverse variations in air–water flow properties in hydraulic jumps with marked roller. Several seminal studies highlighted the existence of large three-dimensional coherent structures in hydraulic jumps (Hoyt and Sellin 1989; Long et al. 1991) (Fig. 1). Fig. 1 illustrates a hydraulic jump in a human-made waterway. Despite a quasi-two-dimensional inflow, large transverse variations were observed as well as large air–water surface structures, with transverse sizes up to three to five times the roller height (Fig. 1). More generally, in the presence of sidewalls, e.g., in a laboratory flume, the development of these large surface features would be hindered by the lateral solid boundaries. In this discussion, the impact of sidewall on the air–water flow properties are discussed in depth and compared with previous work on weak hydraulic jumps with low Froude numbers. Complementary results are presented supporting the comments on the intrinsic limitations of sideview flow visualization approaches. Simply, one needs to be very careful with any definitive conclusion, based on sidewall imaging obtained in laboratory channels.

The sidewall presence affects the air–water flow field because of the combined effects of (a) the *no-flow-through* condition, (b) the *no-slip* condition, and (c) the *zero-void* condition at the wall. With an impervious sidewall, the no-flow-through condition implies that $V_y(y = 0) = 0$ and $v_y'(y = 0) = 0$ at the wall, with V_y the transverse velocity coordinate, v_y' the root-mean square of the transverse component of turbulent velocity, y the transverse coordinate, and $y = 0$ at the sidewall (Fig. 2). At the sidewall itself, the tangential velocity is zero, i.e., the no-slip condition, and this implies $V_x(y = 0) = 0$ and $v_x'(y = 0) = 0$, as well as $V_z(y = 0) = 0$ and $v_z'(y = 0) = 0$, at the wall, with V_x and V_z the longitudinal and vertical velocity coordinates, v_x' and v_z' the root-mean square of the longitudinal and vertical components of turbulent velocity, respectively. At the wall, the bubble concentration is zero because bubbles cannot withstand the very high shear stresses (Madavan et al. 1984; Marie et al. 1991; Chanson 1994). That is, the time-averaged void fraction and bubble count rate at the sidewall respectively satisfy $C(y = 0) = 0$ or 1 and $F(y = 0) = 0$, with C the time-averaged void fraction and F the bubble count rate. The zero-void condition at the sidewall further means zero clustering at the wall, inferring a

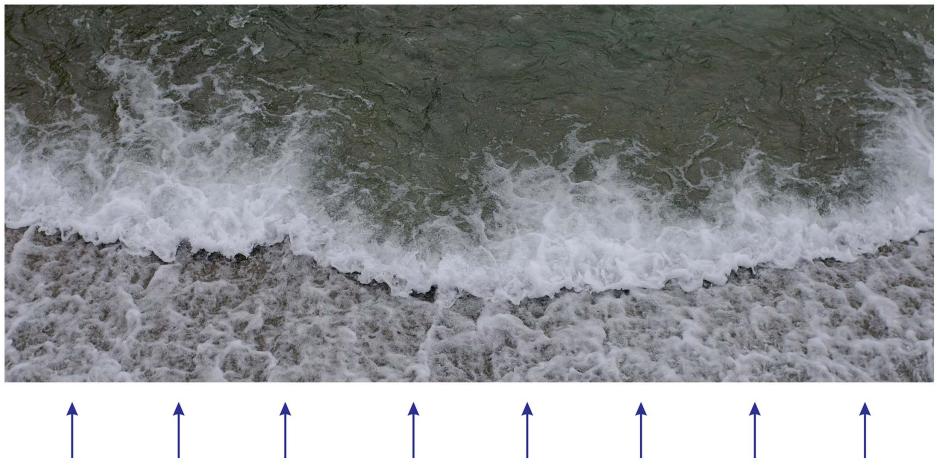

Fig. 1. Three-dimensional air–water surface features in a hydraulic jump along Katashima River, Japan, in October 2012 (shutter speed: 1/250 s). Arrows point in the inflow direction. (Image by Hubert Chanson.)

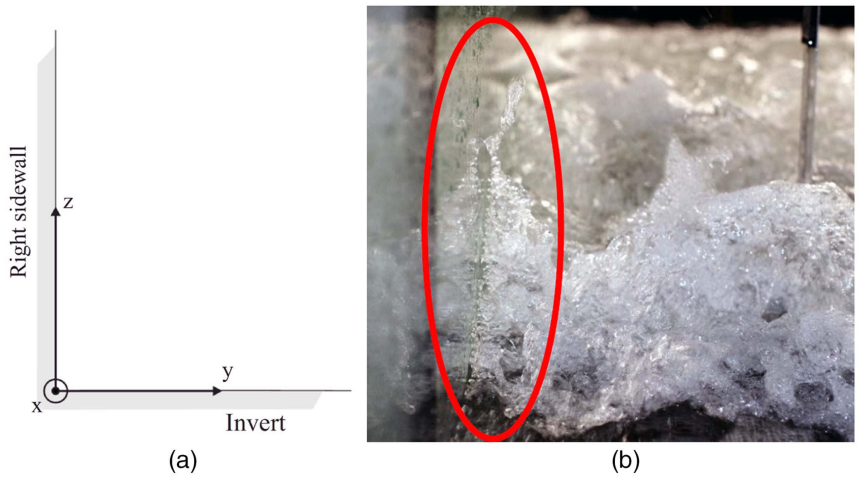

Fig. 2. (a) Definition sketch of channel's coordinate system; and (b) photograph looking downstream toward the impingement perimeter roller toe.

massive difference in bubble–turbulence interplay between the near-wall region and the bulk of air–water breaking roller where high clustering rates are observed (Chanson 2007).

The lateral aeration boundary layer (LABL) introduced by the authors is indeed the sidewall equivalent of the air concentration boundary layer observed at the invert of a smooth spillway and in turbulent boundary layers (Serizawa et al. 1975; Sato et al. 1981; Chanson 1989; Moursali et al. 1995). This sharp gradient in void fraction, bubble count rate, and clustering rate might be conducive of major turbulence modulation, including bubble-induced drag reduction (Marié 1987a; Chanson 1994). Many researchers argued that drag reduction by bubbles is induced by the thickening of the inner region, following Lumley (1977) and others (Madavan et al. 1984; Marié 1987a, b; Ceccio 2010; Murai 2014). Lohse (2018, p.29) suggested that "bubble deformability . . . is responsible for the strong drag reduction" in Taylor-Couette flows. As hinted in earlier works (e.g., Chanson 1994; Moursali et al. 1995), recent direct numerical simulation (DNS) data showed some major difference in bubble deformability between the near-wall region and the outer region (Lu and Tryggvason 2008). Thus, bubble-induced drag reduction might occur at both invert and sidewalls, in view of the occurrence of void fraction boundary layers.

Importantly, the authors' study complemented the earlier works of Wüthrich et al. (2020) in weak hydraulic jumps with breaking roller, undertaken at relatively high Reynolds numbers (Table 1). Both data sets showed important transverse variations in air–water flow properties in the hydraulic jump roller, with large differences between sidewall and centerline air–water hydrodynamic characteristics. The combined results of these two studies were obtained across a broad range of inflow Froude numbers (Table 1) and are thus very general. The findings openly questioned whether data near the sidewalls are truly representative of the behavior in the bulk of the air–water flow. In turn, the results raised the challenges of adverse sidewall effects on image-based techniques, such as bubble image velocimetry (BIV), optical flow (OF), and particle tracking velocimetry (PTV) applied to sidewall photography and cinematography. Typical interactions between air–water surface features and sidewall are illustrated in Fig. 2(b) and the Appendix for weak hydraulic jumps with inflow Froude numbers $Fr_1 = 2.1$–2.4. The flow conditions for these experiments are listed in Table 1 and compared with the original experimental conditions of the authors.

The authors' data were obtained for Froude numbers $Fr_1 = 10.6$–15.1, significantly higher than the experiments of Wüthrich et al. (2022), which focused on hydraulic jumps with inflow Froude numbers $Fr_1 = 2.1$–2.4 and $Re = 1.89$–2.03×10^5. The analogies and differences in the air–water flow properties are reviewed briefly (Figs. 3 and 4). In terms of void fraction distributions, most differences between centerline and sidewall data were observed in the jet aerated region ($0 < y < Y^*$) for both data sets, while the profiles in the recirculation zone were similar. With the bubble count rate, major differences were systematically observed in the jet layer. At both low and high Froude numbers, the sidewall count rate data were much lower than the centerline data [Fig. 3(b)]. This was consistent with Kramer and Valero's (2020) data for $Fr_1 = 4.25$. The interfacial velocity data showed small differences in the jet region, with 15% smaller sidewall velocities. The difference could be partially linked to the smaller recirculation and fewer bubbles detected by

Table 1. Detailed studies of transverse variations of air–water flow properties in hydraulic jump rollers

Reference	Invert slope θ (degrees)	Channel breadth B (m)	Discharge Q (m^3/s)	Inflow depth d_1 (m)	Fr_1	Re_1	Comment
Original article	0	0.40	0.028	0.0133	11.9	5.7×10^4	Pre-aerated inflow
			0.0564	0.0207	15.1	1.41×10^5	
			0.0462	0.0230	10.6	1.16×10^5	
			0.0634	0.0262	11.9	1.59×10^5	
Wüthrich et al. (2022)	0	0.50	0.102	0.097	2.1	2.03×10^5	Partially developed inflow
			0.092	0.084	2.4	1.86×10^5	

Note: Fr_1 = inflow Froude number; and Re_1 = inflow Reynolds number.

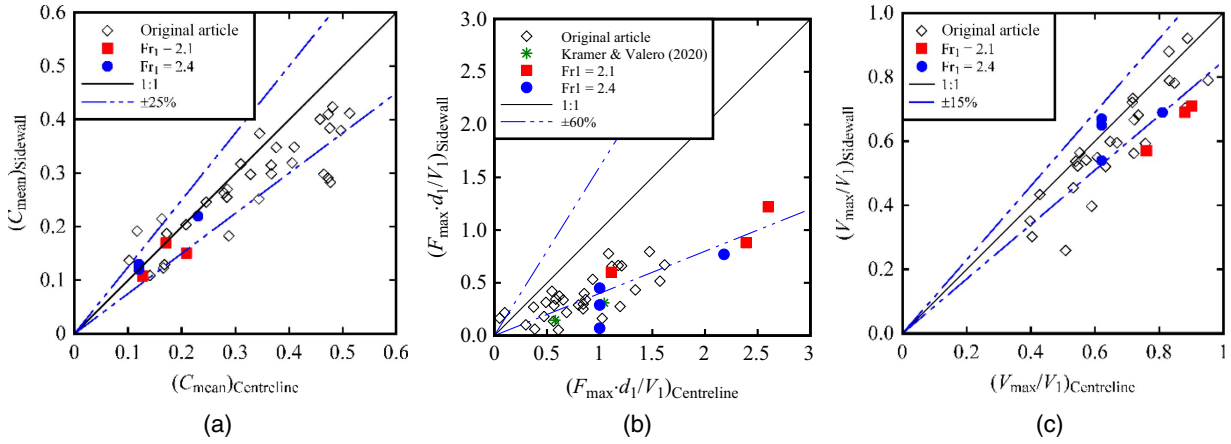

Fig. 3. Comparison of air–water flow data between $Fr_1 = 2.4$ and $Fr_1 = 11.9$ and 15.1.

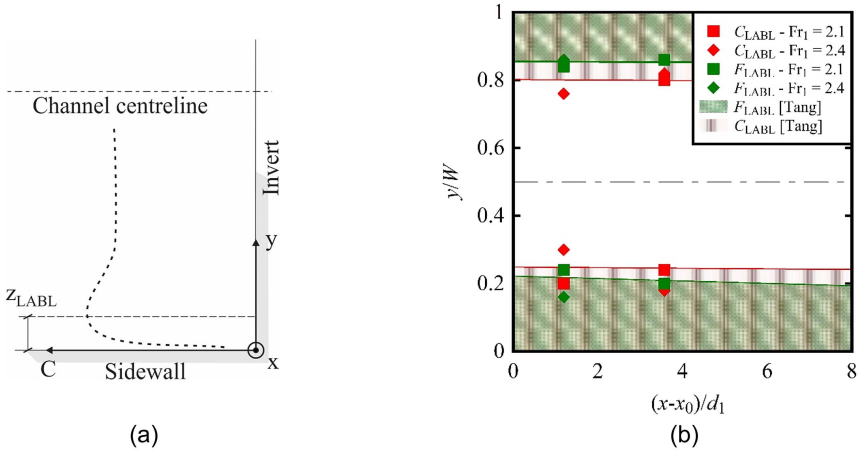

Fig. 4. (a) Definition sketch of the LABL near the sidewalls; and (b) comparison with experimental data by Wüthrich et al. (2022).

the phase-detection probes. Overall, the ratios of the centerline to sidewall air–water flow properties values were comparable for both weak and strong hydraulic jumps (Fig. 3).

In relation to the transverse distributions of air–water flow properties and LABL, three main regions were observed across all Froude numbers as shown in Fig. 4. For $Fr_1 = 2.1$–2.4, the bimodal profile was also observed for $y < Y_{Cmax}$, probably associated with the different behavior in the shear layer, resulting in less pronounced maximum void fraction C_{max} for low Froude numbers. Simply, the authors' work provided some nice evidence of the importance of sidewall effects for high Froude numbers. The findings are shown to be consistent with studies at both low and high Froude numbers, thus extending its validity. This quantitative comparison confirmed, once again, the importance of these findings in the developments of image-processing techniques based on pictures and videos collected near the sidewalls.

Finally, the authors present velocity data sets derived from the adaptive window cross-correlation (AWCC) method. Considering the very high rejection rate of that technique for $C > 0.3$ (Kramer et al. 2019; Chanson 2020), a longer sampling duration could be considered. Furthermore, the differences in rejection rates between centerline and sidewall data sets might affect any direct comparison in terms of the sidewall effects on the air–water velocity field. A comparison in terms of time-averaged velocity data could be developed with those obtained with the more robust traditional cross-correlation technique (Kipphan 1977; Kipphan and Mesch 1978; Crowe et al. 1998). The results would lead to a comprehensive discussion of the pros and cons of the adopted processing method, as well as a more exhaustive interpretation of the effects of sidewalls on the air–water velocity field.

Appendix. Interactions between Hydraulic Jump Roller and Sidewall

Hydraulic jump experiments were undertaken in a rectangular horizontal channel with an internal width $B = 0.50$ m and a test section length of 3.2 m. The horizontal invert was made of high-density polyethylene (HDPE), while the sidewalls were 0.40 m high made of glass to ensure maximum visibility. The inflow conditions were controlled by a vertical gate equipped with a semicircular shape ($\emptyset = 0.3$ m), and the tailwater conditions were set by a vertical overshoot gate located at the downstream end of the test section. Photographic observations of hydraulic jump air–water surface features were recorded in rectangular channels (Table 1). Fig. 5 presents high-shutter photographs of the interactions of the sidewalls with the breaking roller and air–water surface features.

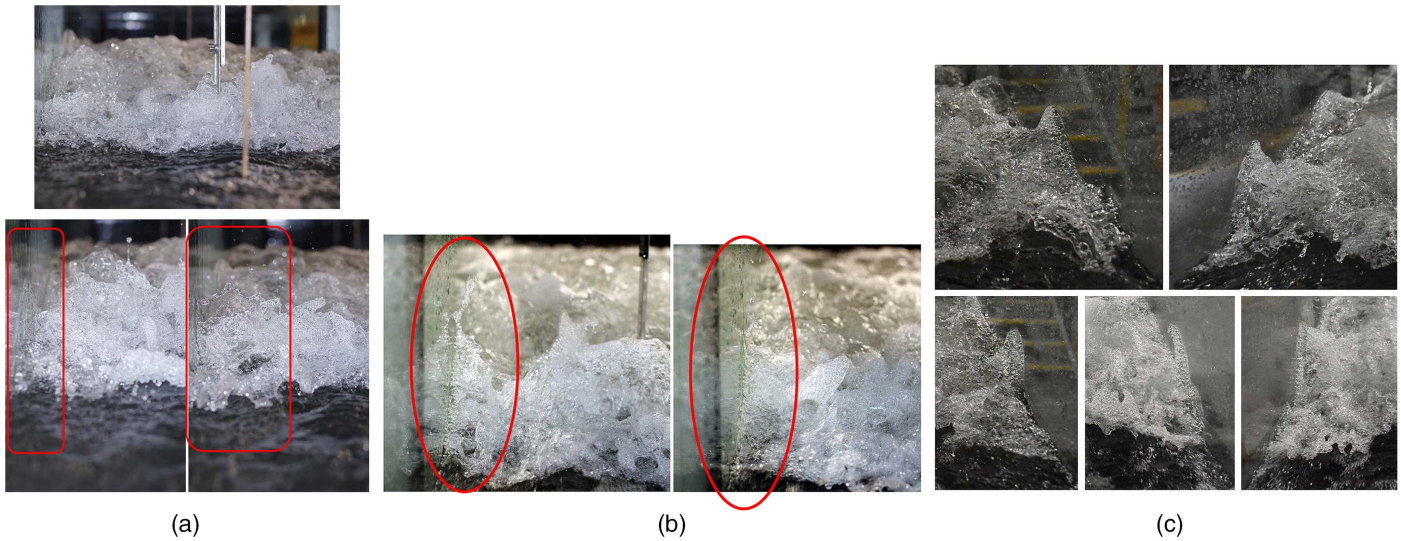

Fig. 5. High-shutter-speed photographs of sidewall effects on air–water flow features in hydraulic jumps with marked roller, looking downstream toward the impingement perimeter roller toe. Circles highlight interactions between air–water surface features and sidewall–flow direction from foreground to background: (a) $Fr_1 = 2.1$, $Re = 2.03 \times 10^5$, $B = 0.50$ m; (b) $Fr_1 = 2.4$, $Re = 1.86 \times 10^5$, $B = 0.50$ m; and (c) further effect of sidewalls on the free-surface flow features ($Fr_1 = 2.1$, $Re = 2.03 \times 10^5$, $B = 0.5$ m).

All photographs were taken from upstream looking downstream at the roller toe and roller surface.

Data Availability Statement

Some or all data, models, or code that support the findings of this study are available from the corresponding author upon reasonable request.

Acknowledgments

H.C. acknowledges earlier helpful exchanges with Professor Oscar Castro-Orgaz, Dr. Carlos Gonzalez, and Dr. Gangfu Zhang. The discussers further acknowledge some fruitful exchanges with Professor Hang Wang.

References

Ceccio, S. L. 2010. "Friction drag reduction of external flows with bubble and gas injection." *Annu. Rev. Fluid Mech.* 42 (Apr): 183–203. https://doi.org/10.1146/annurev-fluid-121108-145504.

Chanson, H. 1989. "Flow downstream of an aerator. Aerator spacing." *J. Hydraul. Res.* 27 (4): 519–536. https://doi.org/10.1080/00221688909499127.

Chanson, H. 1994. "Drag reduction in open channel flow by aeration and suspended load." *J. Hydraul. Res.* 32 (1): 87–101. https://doi.org/10.1080/00221689409498791.

Chanson, H. 2007. "Bubbly flow structure in hydraulic jump." *Eur. J. Mech. B. Fluids* 26 (3): 367–384. https://doi.org/10.1016/j.euromechflu.2006.08.001.

Chanson, H. 2020. "On velocity estimations in highly aerated flows with dual-tip phase-detection probes—A commentary." *Int. J. Multiphase Flow* 132 (5): 103330. https://doi.org/10.1016/j.ijmultiphaseflow.2020.103330.

Crowe, C., M. Sommerfield, and Y. Tsuji. 1998. *Multiphase flows with droplets and particles*. London: CRC Press.

Hoyt, J. W., and R. H. J. Sellin. 1989. "Hydraulic jump as 'mixing layer.'" *J. Hydraul. Eng.* 115 (12): 1607–1614. https://doi.org/10.1061/(ASCE)0733-9429(1989)115:12(1607).

Kipphan, H. 1977. "Bestimmung von Transportkenngrößen bei Mehrphasenströmungen mit Hilfe der Korrelationsmeßtechnik." *Chem. Ing. Tech.* 49 (9): 695–707. https://doi.org/10.1002/cite.330490904.

Kipphan, H., and F. Mesch. 1978. "Flow measurements using transit time correlation." In *Flow measurements of fluids*, 409–416. Amsterdam, Netherlands: North Holand Publications.

Kramer, M., and D. Valero. 2020. "Turbulence and self-similarity in highly aerated shear flows: The stable hydraulic jump." *Int. J. Multiphase Flow* 129 (5): 103316. https://doi.org/10.1016/j.ijmultiphaseflow.2020.103316.

Kramer, M., D. Valero, H. Chanson, and D. B. Bung. 2019. "Towards reliable turbulence estimations with phase-detection probes: An adaptive window cross-correlation technique." *Exp. Fluids* 60 (1): 2. https://doi.org/10.1007/s00348-018-2650-9.

Lohse, D. 2018. "Bubble puzzles: From fundamentals to applications." *Phys. Rev. Fluids* 3 (42): 110504. https://doi.org/10.2469-990X/2018/3(11)/110504(42)).

Long, D., N. Rajaratnam, P. M. Steffler, and P. R. Smy. 1991. "Structure of flow in hydraulic jumps." *J. Hydraul. Res.* 29 (2): 207–218. https://doi.org/10.1080/00221689109499004.

Lu, J., and G. Tryggvason. 2008. "Effect of bubble deformability in turbulent bubbly upflow in a vertical channel." *Phys. Fluids* 20 (6): 040701. https://doi.org/10.1063/1.2911034.

Lumley, J. L. 1977. "Drag reduction in two phase and polymer flows." *Phys. Fluids* 20 (10): 64–71. https://doi.org/10.1063/1.861760.

Madavan, N. K., S. Deutsch, and C. L. Merkle. 1984. "Reduction of turbulent skin friction by microbubbles." *Phys. Fluids* 27 (2): 356–363. https://doi.org/10.1063/1.864620.

Marie, J. L., E. Moursali, and M. Lance. 1991. "A first investigation of a bubbly boundary layer on a flat plate: Phase distribution and wall shear stress measurements." In *Proc., 1st ASME-JSME Fluids Eng. Conf., Turbulence Modification in Multiphase Flows 1991*, 75–80. New York: ASME.

Marié, J. L. 1987a. "A simple analytical formulation for microbubble drag reduction." *Phys. Chem. Hydrodyn.* 8 (2): 213–220.

Marié, J. L. 1987b. "Modelling of the skin friction and heat transfer in turbulence two-component bubbly flows in pipes." *Int. J. Multiphase Flow* 13 (3): 309–325. https://doi.org/10.1016/0301-9322(87)90051-6.

Moursali, E., J. L. Marié, and J. Bataille. 1995. "An upward turbulent bubbly boundary layer along a vertical flat plate." *Int. J. Multiphase Flow* 21 (1): 107–117. https://doi.org/10.1016/0301-9322(94)00059-S.

Murai, Y. 2014. "Frictional drag reduction by bubble injection." *Exp. Fluids* 55 (3): 1–28. https://doi.org/10.1007/s00348-014-1773-x.
Sato, Y., M. Sadatomi, and K. Sekoguchi. 1981. "Momentum and heat transfer in two-phase bubbly flow—II. A comparison between experimental data and theoretical calculations." *Int. J. Multiphase Flow* 7 (5): 179–190. https://doi.org/10.1016/0301-9322(81)90004-5.
Serizawa, A., I. Kataoka, and I. Michiyoshi. 1975. "Turbulence structure of air-water bubbly flows—II. Local properties." *Int. J. Multiphase Flow* 2 (3): 235–246. https://doi.org/10.1016/0301-9322(75)90012-9.
Wüthrich, D., R. Shi, and H. Chanson. 2022. "Hydraulic jumps with low inflow Froude numbers: Air–water surface patterns and transverse distributions of two-phase flow properties." *Environ. Fluid Mech.* 22 (4): 789–818. https://doi.org/10.1007/s10652-022-09854-5.
Wüthrich, D., R. Shi, H. Wang, and H. Chanson. 2020. "Three-dimensional air-water flow properties of a hydraulic jump with low Froude numbers and relatively high Reynolds numbers." In *Proc., 8th IAHR Int. Symp. on Hydraulic Structures*, edited by R. Janssen and H. Chanson. Brisbane, Australia: Univ. of Queensland. https://doi.org/10.14264/uql.2020.583.